

Strain-Path Dependence of $\{10\bar{1}2\}$ Twinning in a Rolled Mg–3Al–1Zn Alloy: Influence of Twinning Model



LINGYU ZHAO, XIAOQIAN GUO, ADRIEN CHAPUIS, YUNCHANG XIN, QING LIU, and PEIDONG WU

In magnesium and its alloys, $\{10\bar{1}2\}$ tension twinning is an important deformation mode and is highly dependent on the strain path. Although the $\{10\bar{1}2\}$ -twinning behavior has been extensively modeled, the effects of twinning models on the predicted results has seldom been compared. In this study, two typical twinning models, predominant twin reorientation (PTR) and twinning-detwinning (TDT), were chosen to simulate the $\{10\bar{1}2\}$ -twinning-predominant deformations of a Mg alloy AZ31 rolled plate, in compression along the transverse direction (TD-c) and in tension along the normal direction (ND-t), and the results were compared with experimental data. In addition to the strain-stress curves in the ND-t and TD-c, six other flow curves were used to determine the material-parameter inputs for the simulations with the elastic visco-plastic self-consistent (EVPSC) model. Compared with the PTR model, the TDT model permits better curve fitting and texture prediction. The PTR model cannot fit the TD-c and ND-t flow stresses simultaneously, whereas the TDT model can. The best-fit parameters for the two models are identical at low strains but diverge somewhat at high strains. The simulated twin volume fractions are similar in the two models, but the predicted textures are significantly different. The PTR model can only reproduce the texture at strains over 5 pct in the TD-c and cannot reproduce the deformed texture in the ND-t. In contrast, the TDT model can reproduce all the experimental textures. To fit both the compression and tension curves well, strong latent hardening of the critical resolved shear stress (CRSS) for $\{10\bar{1}2\}$ twinning by other twinning systems (h'') is necessary. The h'' favors the twin variant with the highest Schmid factor in compression. The h'' increases the CRSS for all $\{10\bar{1}2\}$ twinning systems in tension, but the CRSS for the dominant twinning system remains relatively low in compression.

<https://doi.org/10.1007/s11661-018-4955-y>

© The Minerals, Metals & Materials Society and ASM International 2018

I. INTRODUCTION

PLASTIC deformation of magnesium and its alloys is characterized by easy basal slip with only two independent slip systems and profuse $\{10\bar{1}2\}$ tension twinning, which is the most activated and observed twinning mode. A strong texture with preferential orientation of the $\langle c \rangle$ -axis often develops during plastic forming, *e.g.*, $\langle 0002 \rangle$ parallel to the normal direction (ND) in rolled plates or $\langle 0002 \rangle$ perpendicular to the extrusion direction (ED) in extruded rods.^[1–4] Generally, $\{10\bar{1}2\}$ twinning is initiated by a compressive stress perpendicular to the $\langle c \rangle$ -axis (*e.g.*, in-plane compression along the transverse direction (TD-c) or the rolling direction (RD) of a rolled plate) or a tensile stress parallel to the $\langle c \rangle$ -axis (*e.g.*, through-thickness tension along the ND of a rolled plate). The flow stress of $\{10\bar{1}2\}$ twinning-predominant deformation is characterized by a sigmoid-shaped curve. The role of $\{10\bar{1}2\}$ twinning in plastic deformation includes the subdivision of grains,

LINGYU ZHAO is with the College of Materials Science and Engineering, Chongqing University, Chongqing 400044, China and also with the School of Mechanical Engineering, Yangzhou University, Yangzhou 225127, China. XIAOQIAN GUO is with the State Key Laboratory for Geomechanics and Deep Underground Engineering, China University of Mining and Technology, Xuzhou, Jiangsu 221116, China and also with the School of Mechanics and Civil Engineering, China University of Mining and Technology, Xuzhou, Jiangsu 221116, China. ADRIEN CHAPUIS and QING LIU are with the College of Materials Science and Engineering, Chongqing University. Contact email: achapuis@cqu.edu.cn YUNCHANG XIN is with the College of Materials Science and Engineering, Chongqing University and also with the International Joint Laboratory for Light Alloys, College of Materials Science and Engineering, Chongqing University, Chongqing 400030, China. Contact email: ycxin@cqu.edu.cn PEIDONG WU is with the Department of Mechanical Engineering, McMaster University, Hamilton, ON L8S 4L7, Canada.

Lingyu Zhao and Xiaoqian Guo contributed equally to this paper.

Manuscript submitted April 16, 2018.

Article published online October 26, 2018

rotation of crystallographic orientation, and accommodation of strain along the $\langle c \rangle$ -axis.^[1-7]

There are six different $\{10\bar{1}2\}$ twin variants. The number of twin variants activated strongly depends on the strain path, with more variants activated in through-thickness tension than in-plane compression.^[2,7] In ND tension, several variants have a high Schmid factor and are activated simultaneously, whereas one or two variants often have a significantly higher Schmid factor than the others during in-plane compression, resulting in a limited number of activated twin variants. Consequently, the developed texture components corresponding to the twins are drastically different: ND tension generates an equiaxial texture, with $\langle 0002 \rangle$ lying in the RD-TD plane, whereas compression generates a single $\langle 0002 \rangle$ component, parallel to the compression direction. Generally, at a given strain, the observed twin volume fraction is lower in tension than in compression and twinning exhaustion happens at a higher strain in tension.^[4,8] In addition, a lower stress often exists in ND tension than in TD compression, at a given strain.^[4]

The Schmid law is the main selection mechanism of twin variants,^[5,9,10] but variants with a low Schmid factor may be observed due to strain accommodation.^[11-15] Tension twins may not be observed below ~ 2 pct strain; hence, several authors have erroneously concluded that some slip must occur before twins nucleation.^[6,16] In fact, heterogeneous deformation happens during yielding, and twins tend to propagate from grain to grain, forming “cross-boundary twins,” resulting in a Lüders-like “yield” elongation.^[17,18] Consequently, at low strains, some sample areas are depleted of twins, whereas in other areas, cross-boundary twins proliferate. Sometimes activated twins may not obey the Schmid law.^[12,13] In this case, the strain accommodation among grains plays an important role. The twin fraction is often proportional to the strain, and some acoustic emission and digital-image correlation experiments have confirmed that twinning occurs at the yield point.^[19] The amount of twinning with strain can be measured directly *via* electron backscattered diffraction (EBSD) mapping,^[20] through optical pictures,^[4,16,21] or by indirectly following the texture change.^[22]

Twinning is considered in plastic-deformation modeling of HCP metals. Among others, the visco-plastic self-consistent (VPSC) model^[23] and the elasto-plastic self-consistent (EPSC) model^[24] are particularly adapted to HCP metals. The deformation of AZ31 has been investigated often and successfully modeled with the VPSC (*e.g.*, References 25 and 26) and EPSC (*e.g.*, Reference 27). However, the material parameters diverge greatly from one study to another. The EPSC and VPSC generally use the predominant twin reorientation (PTR) model,^[23] in which the full grain can be reoriented to the most activated twin variant orientation, to keep the number of orientations constant. The twinning-detwinning (TDT) model^[28] has been developed to represent all the twin variants. In the TDT model, each twin variant is represented by a grain with new orientation. In these two models, a threshold twin volume fraction is used to control the twinning events.

In the PTR model, this threshold twin volume fraction allows parent grains to reorient into twin orientations, whereas in the TDT model, it prevents parent grains from further deformation by twinning. This threshold twin volume fraction is usually controlled by two parameters but can be described using only one.^[29] Although this threshold twin volume fraction allows fitting the S-shaped flow curve of $\{10\bar{1}2\}$ twinning-predominant deformation, its parameters are not physically connected, resulting in the stress increase being artificially controlled.

Material parameters are an important input in crystal plasticity models to predict accurately the deformation behavior. However, there is no experimental way to access directly these material parameters; in particular, the critical resolved shear stresses (CRSSs or slip/twin resistance) in single crystals are dramatically different from the ones in polycrystals.^[30] When the material parameters are determined, the hardening of the CRSS for $\{10\bar{1}2\}$ twinning, $\tau_c^{\{10\bar{1}2\}}$, is difficult to characterize, since some studies consider it to be either constant (*e.g.*, References 31 through 34), decreasing (*e.g.*, References 18 and 35 through 37), or increasing (*e.g.*, References 25, 27, 38 and 39). Since through-thickness tension promotes several $\{10\bar{1}2\}$ twin variants, it is possible that they interact with each other and harden the threshold twinning stress, whereas with in-plane compression, no such hardening is expected. The hardening of the twinning systems can be modeled *via* a latent-hardening coefficient for twinning, h'' , higher than 1. A previous study used $h'' = 10$ to model both tension and compression experiments,^[39] but the effect of h'' was not elucidated.

Although the VPSC-TDT and VPSC-PTR models have shown good capacity for fitting the stress-strain curves of twin-dominated deformation,^[5,25,31,32,35,40-42] they may predict a significantly different amount of twinning and texture evolution. The material parameters can be influenced by the twinning model because the PTR model rapidly reorients some grains into twins, whereas the TDT model incorporates all the twin variants since their nucleation. The PTR model has often been used to simulate twinning during in-plane compression^[5,25,31,32,35,41,42] but has never (to the best of our knowledge) been used to simulate ND tension. The twinning-dominated deformation has been experimentally investigated at low strain in several studies (*e.g.*, Reference 2), but texture evolution has seldom been modeled at low strain levels. Texture is generally simulated and compared with experimental data above twinning exhaustion (*e.g.*, References 5, 7, 25, 35, 43 and 44), with a few exceptions (References 34, 36 and 45).

Until now, no study has reported on a systematic comparison between PTR and TDT modeling for $\{10\bar{1}2\}$ twinning-predominant deformation. In the present work, two types of $\{10\bar{1}2\}$ twinning-predominant deformations (ND tension and TD compression) were simulated using both the EVPSC-PTR and EVPSC-TDT models, with the aim of illustrating the exact difference between them for simulating the strain-path dependence of twinning behavior in Mg

alloys. In addition, the effect of the latent-hardening modulus for tension twinning on predictions of twinning behavior was also addressed.

II. EXPERIMENTS AND METHODS

A. Experimental Procedures

The initial material was a 60-mm-thick hot-rolled plate of Mg-alloy AZ31 (nominal contents of 3 pct Al, 1 pct Zn, and 0.6 pct Mn), annealed for 2 hours at 400 °C. A few specimens were cut with the loading direction along the ND, TD, and RD, and at a 45-deg angle between the RD and ND, and deformed to fracture in uniaxial tension and compression, at an initial strain rate, $\dot{\epsilon} = 0.0005 \text{ s}^{-1}$, at room temperature (the test details have been previously described^[39]). For the present study, specific through-thickness tension (tension along the normal direction (ND-t)) and in-plane compression (TD-c) samples were deformed to different strains (1, 2, 3, 4, 5, and 10 pct). The ND-t samples were dog-bone shaped, with a 25-mm gage length and 6-mm diameter. The TD-c samples were cylinders with a 15-mm height and 9-mm diameter. An extensometer was used to measure strain during the tension tests.

The initial (*i.e.*, annealed AZ31 plate) and deformed microstructures at different strains were examined by EBSD, using a TESCAN MIRA 3 SEM equipped with an Oxford Instruments-HKL Technology Nordlys EBSD system. Preliminary sample preparation consisted of manual and electropolishing with AC2 solution, at 20 V for 1.5 minutes. Deformed samples were cut at midheight and the analyzed surface was normal to the loading direction. The texture was measured on $0.5 \times 0.5 \text{ mm}^2$ maps with a $1\text{-}\mu\text{m}$ step size. For each sample, more than two maps were used to measure the texture. All EBSD data were processed using Channel 5. The twin volume fraction was measured by manually selecting the twins on the EBSD maps.

B. Constitutive Models

The numerical simulations are based on the elastic visco-plastic self-consistent (EVPSC) model of Wang *et al.*,^[46] with the PTR scheme introduced by Lebensohn *et al.*,^[47] and the TDT description proposed by Wang *et al.*^[28,40] In this section, the EVPSC-PTR and EVPSC-TDT models are briefly summarized, for definition and notation. Details can be found in previous publications by Lebensohn *et al.*^[47] and Wang *et al.*^[28,40,46]

The plastic deformation of a crystal is assumed to be due to crystallographic slip and twinning in a crystallographic system (s^α, n^α), with s^α and n^α being the slip/twinning direction and normal to the slip/twinning plane, respectively, for system α . For Mg alloys, the basal $\langle a \rangle$ ($\{0001\} \langle 11\bar{2}0 \rangle$), prismatic $\langle a \rangle$ ($\{10\bar{1}0\} \langle 11\bar{2}0 \rangle$), and pyramidal $\langle c + a \rangle$ ($\{11\bar{2}2\} \langle 11\bar{2}3 \rangle$) slip systems are considered, as well as the $\{10\bar{1}2\} \langle 1011 \rangle$ tension twinning and $\{10\bar{1}1\} \langle 10\bar{1}2 \rangle$ compression twinning systems.

For both slip and twinning, the driving force for the shear rate, $\dot{\gamma}^\alpha$, is the resolved shear stress, τ^α . For slip,

$$\dot{\gamma}^\alpha = \dot{\gamma}_0 \left(\frac{\tau^\alpha}{\tau_c^\alpha} \right)^{1/m} \text{sgn}(\tau^\alpha) \quad [1]$$

For twinning,

$$\dot{\gamma}^\alpha = \begin{cases} \dot{\gamma}_0 \left| \frac{\tau^\alpha}{\tau_c^\alpha} \right|^{1/m} & \tau^\alpha > 0 \\ 0 & \tau^\alpha < 0 \end{cases} \quad [2]$$

where $\dot{\gamma}_0$ is a reference shear rate ($\dot{\gamma}_0 = 0.001$), τ_c^α is the CRSS, and m is the strain-rate sensitivity ($m = 0.05$). The reference shear rate is chosen to be equal to the strain rate along the loading direction $\dot{\epsilon} = \dot{\gamma}_0 = 0.001 \text{ s}^{-1}$ (boundary condition imposed in the velocity gradient tensor), and the strain-rate-sensitivity parameter is relatively low because magnesium is nearly rate insensitive at room temperature under quasi-static deformation. Doing so, the CRSSs are strain rate independent and the strain-rate-sensitivity parameter m loses its physical meaning but allows easy convergence of the EVPSC.

In the PTR approach, the amount of shear strain, γ^α , accommodated by the α^{th} twin variant within a grain, is monitored, and the corresponding twin volume fraction, f^α , is computed by

$$f^\alpha = \gamma^\alpha / \gamma^{\text{tw}} \quad [3]$$

where γ^{tw} denotes the characteristic twinning shear of the mode in question.

Parent grains can be reoriented into a twin before the grain is totally twinned (*i.e.*, before the sum of twin variant volume fraction is 1). Both the PTR and TDT models introduce two statistical variables: accumulated twin fraction, V^{acc} , and effective twin fraction, V^{eff} . More specifically, V^{acc} and V^{eff} are the weighted volume fractions of the twinned region and twin-terminated grains, respectively. In the PTR, twin-terminated grains are grains already reoriented into twins, whereas in the TDT, they are grains in which no more twinning is allowed. The threshold volume fraction, V^{th} , is defined as

$$V^{\text{th}} = \min \left(1, A_1 + A_2 \frac{V^{\text{eff}}}{V^{\text{acc}}} \right) \quad [4]$$

where A_1 and A_2 are two material constants. At each incremental step, the PTR selects randomly some parent grains and reorients them into the corresponding twin variant of highest twin volume fraction until Eq. [4] is verified. The advantage of the PTR approach is that it is computationally efficient. There is no increase in the number of grains that must be tracked by the code. Multiple twinning is also allowed; *i.e.*, a twin can deform by twinning and be reoriented into another twin. However, the disadvantage is that not every activated twin variant is present in the final simulated “microstructure,” since only the predominant twin variant is respected by the model. This could be significant when many variants are observed to occur.

The TDT model assumes that a grain has four potential operations associated with twinning and detwinning. Operation A is twin nucleation and initiates a twin band or “child.” Operation B is propagation of the child into the parent. Operations A and B increase the twin volume fraction and, thus, correspond to twinning. Operation B can take place both in the parent and the twin, so the twin can deform by twin growth. Operation C is propagation of the parent into the child. Operation D splits the twin band and decreases the twin volume fraction through retwinning. Operations C and D decrease the twin volume fraction and, thus, correspond to detwinning. The TDT model treats the new twin band (child) as a new grain, and all six extension twin variants are potentially present. Since it is rare that a grain can be fully twinned, the threshold twin volume fraction defined in Eq. [4] is also used in the TDT model, to terminate twinning. Although it was not employed in the present work, a single-parameter version of the TDT model has been previously developed by Qiao *et al.*^[29]

Unlike the PTR model, where the original grain orientation is suddenly transformed to the twin orientation, the TDT model generates a new grain every time a new twin variant is activated. The orientation of the twin is initially related to that of the parent through the crystallographic twin relationship, and the volume fraction associated with the twin is updated at every straining step in which the twin variant is activated. However, this approach suffers from a computational penalty for the grain proliferation. In principle, even considering only the $\{10\bar{1}2\}$ tension twinning and the $\{10\bar{1}1\}$ compression twinning mode, a parent grain could potentially become 13 grains (parent plus six extension twins plus six compression twins). In the TDT model, evolution of the twin volume fraction associated with the twinning system, β , is governed by

$$\dot{f}^\beta = f^0 (\dot{f}^{\beta A} + \dot{f}^{\beta C}) + f^\beta (\dot{f}^{\beta B} + \dot{f}^{\beta D}) \quad [5]$$

where f^0 is the volume fraction of the parent, *i.e.*, $f^0 = 1 - f^{tw} = 1 - \sum_{\beta} f^\beta$, and the superscripts *A*, *B*, *C*,

and *D* represent the respective operations. In the present approach, multiple twinning is not considered. In the present study, operations C and D are not expected to occur because no strain-path change is modeled. Twins can deform only by growth and slip.

For both slip and twinning, evolution of the CRSS, τ_c^α , is given by

$$\dot{\tau}_c^\alpha = \frac{d\hat{\tau}^\alpha}{d\Gamma} \sum_{\chi} h^{\alpha\chi} |\dot{\gamma}^\chi| \quad [6]$$

where $\Gamma = \sum_{\beta} \int |\dot{\gamma}^\beta| dt$ is the accumulated shear strain in

the grain and $h^{\alpha\chi}$ represents the latent-hardening coupling coefficients, which empirically account for the obstacles in system α , associated with system χ . $\hat{\tau}^\alpha$ is the threshold stress and is characterized as follows:

$$\hat{\tau}^\alpha = \tau_0^\alpha + (\tau_1^\alpha + \theta_1^\alpha \Gamma) (1 - \exp(-\frac{\theta_0^\alpha}{\tau_1^\alpha} \Gamma)) \quad [7]$$

Here, τ_0 , θ_0 , θ_1 , and $\tau_0 + \tau_1$ are the initial CRSS, initial hardening rate, asymptotic hardening rate, and back-extrapolated CRSS, respectively.

The response of a polycrystal comprised of many grains is obtained by applying the self-consistent approach. Various self-consistent schemes have been proposed. Wang *et al.*^[46] demonstrated that the predicted response of a polycrystal is very sensitive to the self-consistent scheme employed. Wang *et al.*^[32] also evaluated various schemes used in self-consistent modeling of a Mg alloy and found that the *Affine* self-consistent scheme gave the best overall performance among all the approaches examined. Therefore, the *Affine* self-consistent scheme is employed in the present study.

III. RESULTS AND DISCUSSION

A. Traditional Modeling

In this section, for all the deformation modes, self- and latent hardening for a slip or twin system by the other systems (of the same mode) are assumed to be the same. This means that the CRSS for all the systems of a given mode are the same in each grain. This assumption is generally made as self- and latent hardenings are indifferentiable. To model the plastic deformation of the AZ31 plate, the EVPSC-PTR and EVPSC-TDT models are used. The modeling procedure to fit the parameters followed a rationale described previously,^[48] with a few compromises. The material parameters were first determined to fit ND compression, TD compression (*i.e.*, TD-c), and TD tension. Then, the eight available stress-strain curves were simulated. If the behavior was not reproduced satisfactorily, the material parameters were further adjusted and rechecked. In this section, it has been assumed that all self- and latent-hardening coefficients were $h^{ss'} = 1$, except h^{st} , for slip associated with $\{10\bar{1}2\}$ twinning. As in previous studies, additional hardening due to twin boundaries or dislocation transmutation^[36,49,50] is taken into account by the latent-hardening coefficient of twinning so that the twinning activity hardens the slip modes at an increased rate ($h^{st} > 1$). The h^{st} is also expected to be higher in tension, where several twin variants generate more twin boundaries, than in compression, where one twin can occupy the entire matrix. Since self- and latent-hardening coefficients are indistinguishable, for simplicity, both the self- and latent-hardening coupling coefficients for all slip modes are $h^{ss'} = 1$. Only in a very few studies have different latent-hardening coefficients for slip modes, $h^{ss'}$, been considered.^[35,51]

The material parameters for the EVPSC-PTR and the EVPSC-TDT models are listed in Tables I and II, respectively. In this section, the parameter $q = h^{tt} = 1$ and the corresponding simulated χ curves, compared with the experimental ones, are plotted in Figures 1 and 2.

Table I. Material-Parameter Inputs for the EVPSC-PTR Model; h^{st} represents the Latent-Hardening Coefficients for Slip Systems Associated with the $\{10\bar{1}2\}$ Twinning Systems

Mode	τ_0 (MPa)	τ_1 (MPa)	θ_0 (MPa)	θ_1 (MPa)	h^{st}	A_1	A_2
Basal Slip	10	1	100	25	1	—	—
Prismatic Slip	67	50	600	20	2	—	—
Pyramidal Slip	90	70	1500	25	1.5	—	—
$\{10\bar{1}2\}$ Twinning	25	1	200	130	q	0.7	0.3
$\{10\bar{1}1\}_t$ Twinning	140	5	200	70	4	0.01	0.04

Table II. Material-Parameter Inputs for the EVPSC-TDT Model; h^{st} Represents the Latent-Hardening Coefficients for Slip Systems Associated with the $\{10\bar{1}2\}$ Twinning Systems

Mode	τ_0 (MPa)	τ_1 (MPa)	θ_0 (MPa)	θ_1 (MPa)	h^{st}	A_1	A_2
Basal Slip	10	1	10	0	1	—	—
Prismatic Slip	67	53	600	30	1.2	—	—
Pyramidal Slip	90	75	1600	0	1.5	—	—
$\{10\bar{1}2\}$ Twinning	25	1	200	130	q	0.7	0.3
$\{10\bar{1}1\}$ Twinning	150	5	200	50	1	0.2	0.2

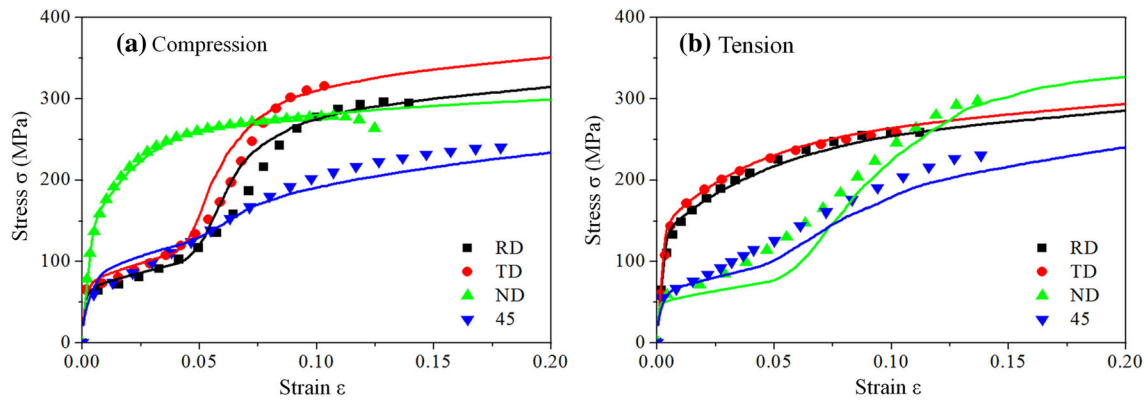


Fig. 1—Simulations with the EVPSC-PTR model and parameters from Table I and $q = 1$; measured (symbols) and simulated (lines) true stress-strain curves under (a) uniaxial compression and (b) uniaxial tension along the ND, TD, and RD and at a 45-deg angle between the RD and ND.

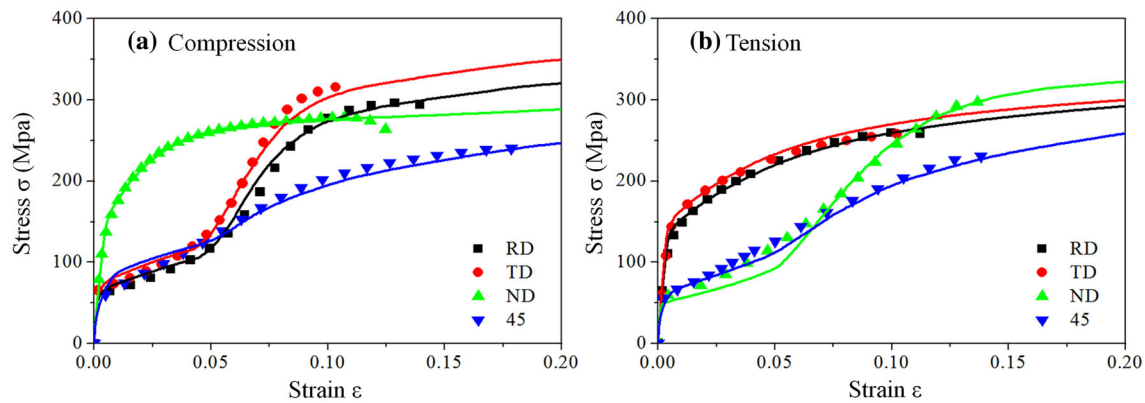


Fig. 2—Simulations with the EVPSC-TDT model and parameters from Table II and $q = 1$; measured (symbols) and simulated (lines) true stress-strain curves under (a) uniaxial compression and (b) uniaxial tension along the ND, TD, and RD and at a 45-deg angle between the RD and ND.

The $\{10\bar{1}1\}$ compression twinning is included, and its CRSS is fitted to have a non-negligible amount of twinning, as observed in both compression^[42] and tension.^[52] With the EVPSC-PTR model, it is necessary to input a strong latent hardening, h^{st} , for $\{10\bar{1}1\}$ twinning by $\{10\bar{1}2\}$ twinning to prevent excessive $\{10\bar{1}2\} - \{10\bar{1}1\}$ twinning and allow for a high flow stress. The parameters A_1 and A_2 , which have different meanings in the PTR and TDT models, are fixed to “physically representative” values before the curve-fitting procedure. Tension twins can rapidly consume the entire grain; hence, A_1 is fixed at a high value. In contrast, contraction twins rapidly saturate and soften the material.

When fitting the in-plane compression curves (TD-c and RD-c), it is necessary to include a latent hardening, h^{st} , for pyramidal $\langle c + a \rangle$ slip by $\{10\bar{1}2\}$ twinning, so that when the twins deform (*i.e.*, $\varepsilon > 0.1$), the simulated flow stress increases sufficiently. When fitting the through-thickness tension curve (ND-t), it is necessary to include a latent hardening, h^{st} , for prismatic slip by $\{10\bar{1}2\}$ twinning, so that when the twins deform (*i.e.*, $\varepsilon > 0.12$), the simulated flow stress increases sufficiently. It is common to have a higher latent hardening, h^{st} , by $\{10\bar{1}2\}$ twinning (*e.g.*, References 31, 39 and 53). We can note that the h^{st} values are different for the two models.

The twin-induced hardening can be evaluated. When $h^{st} = 1$ is used for pyramidal $\langle c + a \rangle$ and prismatic slip, the EVPSC-PTR simulated TD-compression flow stress at $\varepsilon = 0.1$ is $\sigma = 278$ MPa instead of 313 MPa. The EVPSC-TDT simulated TD-compression flow stress at $\varepsilon = 0.1$ is $\sigma = 278$ MPa. The ND-tension EVPSC-PTR simulated flow stress at $\varepsilon = 0.13$ is $\sigma = 259$ MPa instead of 295 MPa. The ND-tension EVPSC-PTR simulated flow stress at $\varepsilon = 0.13$ is $\sigma = 289$ MPa. Consequently, the $h^{st} = 1.5$ for pyramidal $\langle c + a \rangle$ slip increases the TD-c flow stress after twinning exhaustion by 35 MPa, with both the PTR and TDT schemes. However, the $h^{st} = 2$ for prismatic slip increases the ND-t flow stress after twinning exhaustion by 36 MPa with the EVPSC-PTR model, and the $h^{st} = 1.2$ for prismatic slip increases the ND-t flow stress after twinning exhaustion by 6 MPa. It is clear that the parameters and modeled twinning behavior have many similarities in compression when the PTR and TDT models are used, but in tension, the two twinning models strongly affect the modeling. Consequently, the h^{st} values depend on the chosen material parameters^[7,39] and on the twinning models.

In the EVPSC-PTR model, the addition of an asymptotic hardening rate, θ_1 , to the threshold stress for basal slip is justified, to prevent the simulated flow stress of 45-c and 45-t from being too low at high strains. The “effective twin fraction” is lower than the “accumulated twin fraction,” but lowering the threshold value, A_1 , does not significantly increase the flow stress at high strains.

It appeared that it was impossible to perfectly fit all the curves. The PTR model does not allow for modeling of the transition from twinning of the matrix to twin deformation (as observed by Brown *et al.*^[5]), and the

twin-induced hardening is premature in compression but delayed in tension. The parameters used are compromises, resulting in moderate overestimation of the simulated flow stress in the in-plane compression (and in the 45-deg compression) at low strains and large underestimation of the flow stress in the through-thickness tension (and, to a lower extent, in the 45-deg tension).

B. Improved Modeling

In modeling the stress-strain curves, the biggest discrepancy is observed in the ND-tension curve, which is largely underestimated. A recent study showed that input of latent hardening h^{st} for $\{10\bar{1}2\}$ twinning systems by $\{10\bar{1}2\}$ twins resulted in a lower discrepancy and tended to satisfactorily fit all the stress-strain curves.^[39] In fact, the parameter, q , is in the matrix, h^{st} , described by Eq. [8], which allows for increasing the CRSS, $\tau_c^{\{10\bar{1}2\}}$, for each twinning system, at a higher rate than that for self-hardening. The present underlying physical motivation is that different twinning variants lie on different planes, and when one twin variant is present, the others have less space to grow in the parent grain; hence, their nucleation and growth are more difficult. Since more twin variants are generally present in tension than in compression,^[2,7] a latent-hardening coefficient, $q > 1$, should increase $\tau_c^{\{10\bar{1}2\}}$ of the active twinning systems more in tension than in compression. Several attempts were conducted for the present study, and the best-fit parameters, shown in Table II with $q = 5$, permitted the curve fitting shown in Figure 3.

$$h^{st} = \begin{bmatrix} 1 & q & q & q & q & q \\ q & 1 & q & q & q & q \\ q & q & 1 & q & q & q \\ q & q & q & 1 & q & q \\ q & q & q & q & 1 & q \\ q & q & q & q & q & 1 \end{bmatrix} \quad [8]$$

Figure 4 shows the experimental and simulated curves with the four sets of parameters described in Tables I and II for the PTR and TDT models, respectively, with $q = 1$ and 5. The ND-t flow-stress curve, simulated with the EVPSC-PTR model, deviates a lot from the experimental curves. As compared with $h^{st} = q = 1$, the parameter $q = 5$ marginally increases the TD-compression flow stress at strain $\varepsilon < 0.04$. However, with $q = 5$, the simulated ND-tension flow stress increases significantly at $0.01 < \varepsilon < 0.07$ in the two twinning models. With the parameters from Table II and $q = 5$, the EVPSC-TDT modeled curves provide the best-fit simulations.

As compared with a previous study,^[39] in which the coefficient $h^{st} = 10$ was employed, the CRSS parameters for $\tau_c^{\{10\bar{1}2\}}$ are different: in the present study, τ_1 is negligible, whereas the asymptotic hardening, θ_1 , is significantly higher. The current parameters are preferred to decrease the simulated flow stress at low strains in the in-plane compression (*i.e.*, TD-c).

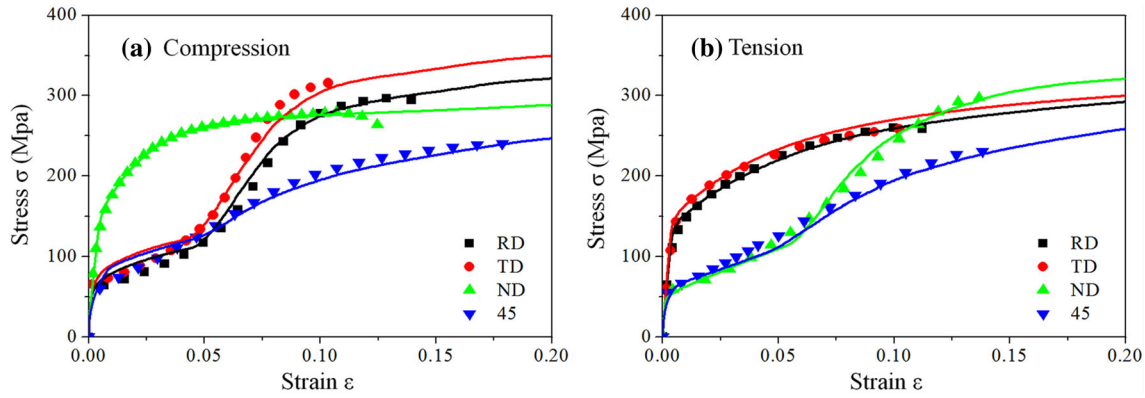


Fig. 3—Simulations with the EVPSC-TDT model and parameters from Table II and $q = 5$; measured (symbols) and simulated (lines) true stress–strain curves under (a) uniaxial compression and (b) uniaxial tension.

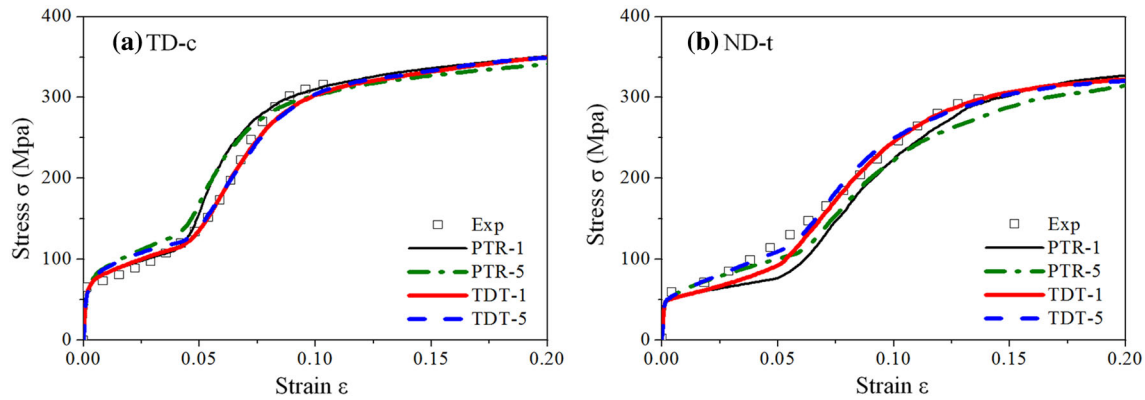


Fig. 4—Measured (symbols) and simulated (lines) stress–strain curves with the EVPSC-PTR and EVPSC-TDT models, with $q = 1$ and 5 (parameters in Tables I and II), under (a) TD compression and (b) ND tension.

C. Twinning Activity and Twin Volume Fraction

Figure 5 displays the deformation-system activity for each twinning model and parameter q . All models and parameters show that $\{10\bar{1}2\}$ twinning dominates TD compression at low strains but extinguishes rapidly (at $\varepsilon < 0.1$). In contrast, ND tension is dominated by basal slip, whereas $\{10\bar{1}2\}$ twinning continues until $\varepsilon \approx 0.15$. There are a few small but observable differences in relative activity between the EVPSC-PTR and EVPSC-TDT models, but the latent-hardening parameter, q , seems to have a limited effect. The simulated activity above $\varepsilon \approx 0.10$ confirms that twin-terminated grains (or tension twins) deform by basal and pyramidal $\langle c + a \rangle$ slip in compression and by prismatic and basal slip in tension. Among others, Agnew *et al.*^[25] simulated the relative activity in in-plane compression with the VPSC-PTR for a similarly textured AZ31 alloy: the relative activity for tension twinning at low strain reached 75 pct. With the VPSC-CG model, Proust *et al.*^[35] estimated it to be about 95 pct. The relative activity of tension twinning is much lower in the present study, which may be due to the lower τ_c^{basal} assessed presently.

The differences in $\{10\bar{1}2\}$ twinning activity are better observable in terms of the accumulated twin volume

fractions, displayed in Figure 6. The twin volume fractions measured directly from the EBSD map are also reported in Figure 6. Since the deformation is not homogeneous, the measurements have to be interpreted carefully. These results are relatively close to those of Hong *et al.*,^[4] showing faster twinning in compression than in tension. However, the shapes of the curves are different: experimentally, almost no tension twins are observed at very low strain ($\varepsilon = 1$ pct). Although the twin volume fraction measured by Hong *et al.* showed a sigmoid-shaped increase *vs* strain in ND tension, both the present measurements (despite the heterogeneous deformation) and the simulations show a linear increase in the twin volume fraction. Hence, the total twin volume fraction is determined largely by the strain, as observed in compression.^[17] Experimentally, $\{10\bar{1}2\}$ twins are seldom observed by EBSD at low strains^[6,54] and seem to nucleate at ~ 2 pct plastic strain. However, some studies have shown that twins nucleate at the onset of plastic deformation.^[17,19,55] Models tend to overestimate the tension twin volume fraction at low strain, except when some probabilistic functions are used to dictate twin nucleation.^[56] The present EVPSC model is not an exception and moderately overestimates the twin volume fraction.

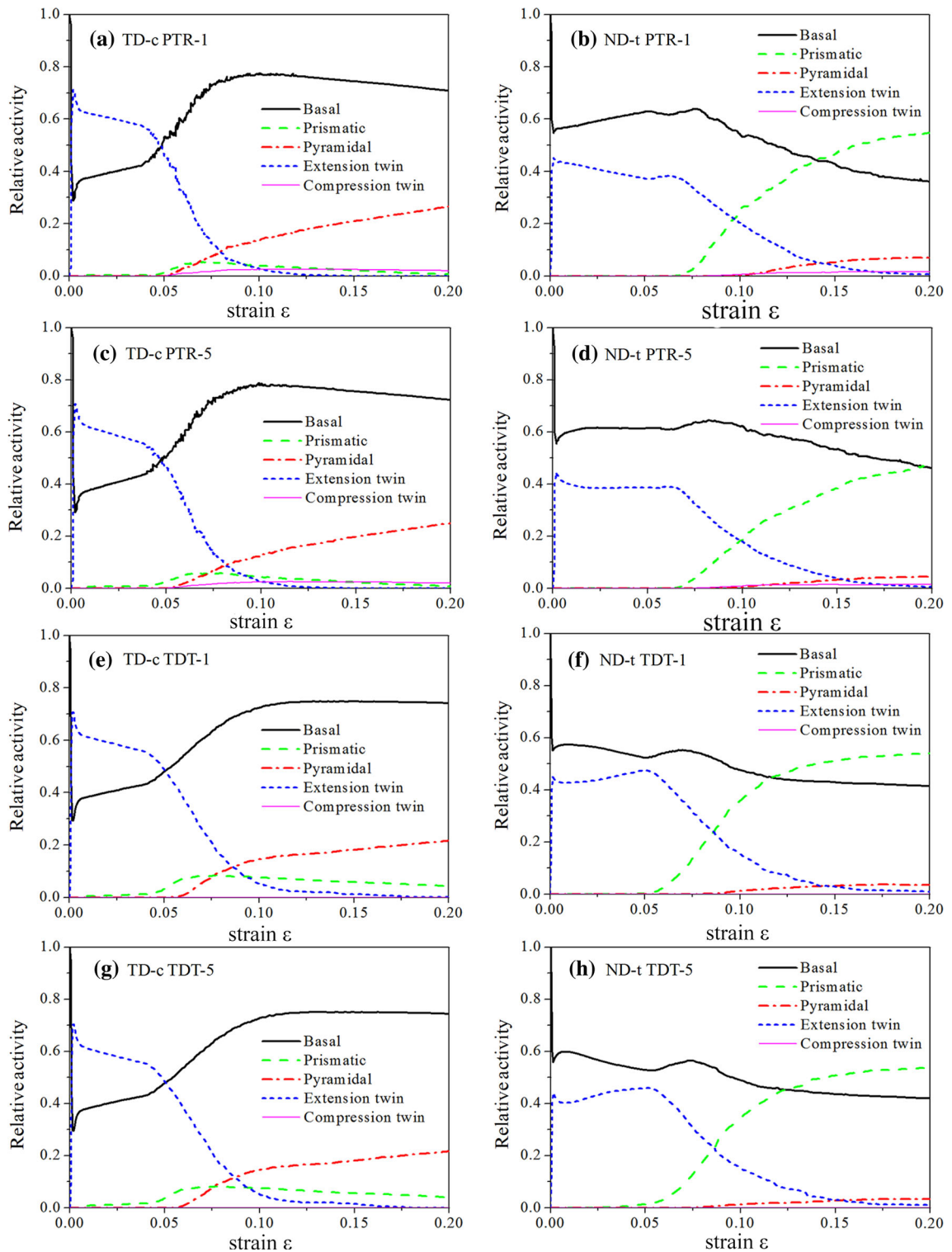


Fig. 5—Relative activity of slip/twinning in TD compression (left) and ND tension (right), with the EVSPC-PTR model, with (a) and (b) $q = 1$ and (c) and (d) $q = 5$, and the EVSPC-TDT model, with (e) and (f) $q = 1$ and (g) and (h) $q = 5$ (parameters in Tables I and II).

D. Texture Evolution

The texture was measured from the EBSD maps (surface $\sim 0.5 \times 0.5 \text{ mm}^2$) and simulated with the EVSPC-PTR and EVSPC-TDT models using the parameters in Tables I and II, respectively. The results

at different strains are displayed in Figures 7 through 10. The loading direction is in the middle of the pole figures, to fit with the observed surface.

TD compression makes the $\langle c \rangle$ -axis reorient from the ND to TD due to $\{10\bar{1}2\}$ twinning (Figure 7). Since

grain reorientation into twin is delayed in the PTR model, the texture component corresponding to the tension twins does not appear in the predicted texture below $\varepsilon = 4$ pct. In contrast, the TDT model can suitably reproduce the texture at low strains. At $\varepsilon = 1$ pct, the predicted texture component corresponding to twinning is at least 2 times higher than the measured one. However, as stated previously, the deformation is heterogeneous at low strains and a large area on the EBSD map was twin free. In comparison, Knezevic *et al.*^[6] hardly observed tension twins at $\varepsilon = 2.5$ pct in-plane compression, and the texture component

$\langle c \rangle \parallel \text{ND}$ was not visible until $\varepsilon = 4$ pct. At high strains, the parent-grain orientation intensity decreases and, experimentally, almost disappears at 10 pct. In the simulations, a few parent orientations remain close to the ND. With the PTR model, these components rotate about 20 deg toward the TD, whereas they remain parallel to the ND with the TDT model. The reason may be that in the EVPSC-PTR, parent grains deform continuously by basal slip and twinning and basal slip makes $\langle c \rangle$ rotate toward the compression direction.^[57] On the opposite, with the EVPSC-TDT, parent grains are prevented to deform after twinning exhaustion so they have to deform by basal and pyramidal $\langle c + a \rangle$ slip; the latter makes $\langle c \rangle$ rotate toward the extension direction.^[57] The $\langle c \rangle$ -axes close to the TD (corresponding to $\{10\bar{1}2\}$ twins) also tilt somewhat toward the RD, both experimentally and in all the simulations.

A strong preferential $\{10\bar{1}0\} \parallel \text{ND}$ orientation is predicted by the PTR model at $\varepsilon = 5$ pct, and this tendency (although less strong) is also observed in the experimental and simulated pole figures (Figure 8). Knezevic *et al.*^[6] also experimentally observed a strong $\{10\bar{1}0\} \parallel \text{ND}$ component above $\varepsilon = 4$ pct.

In ND tension, the effective tension twin volume fraction is too low within the PTR model and significant grain reorientation does not occur below $\varepsilon = 5$ pct (Figure 9). However, at $\varepsilon = 10$ pct, the PTR clearly favors $\langle c \rangle \parallel \text{RD}$ and the remaining parent grains rotate toward the reduction direction (RD in this case).

The measured twin volume fraction is somewhat lower than the one predicted with the EVPSC-TDT model below $\varepsilon = 2$ pct, which is also visible on the pole figures. However, at $\varepsilon = 3$ pct, both the experimental

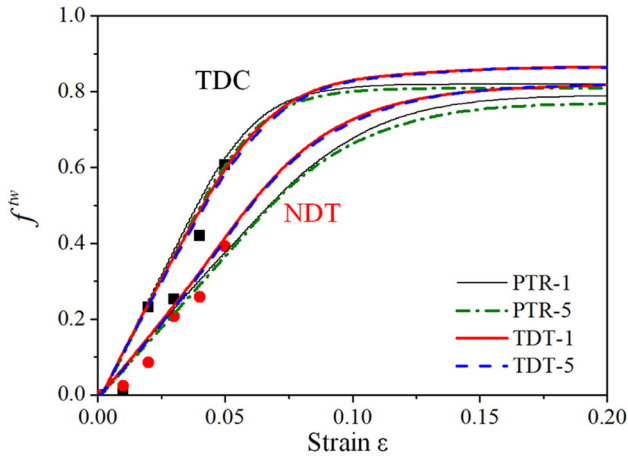


Fig. 6—Measured (symbols) and simulated (lines) twin volume fractions in TD compression and ND tension, with the EVPSC-PTR and EVPSC-TDT models, and with $q = 1$ and 5 (parameters in Tables I and II).

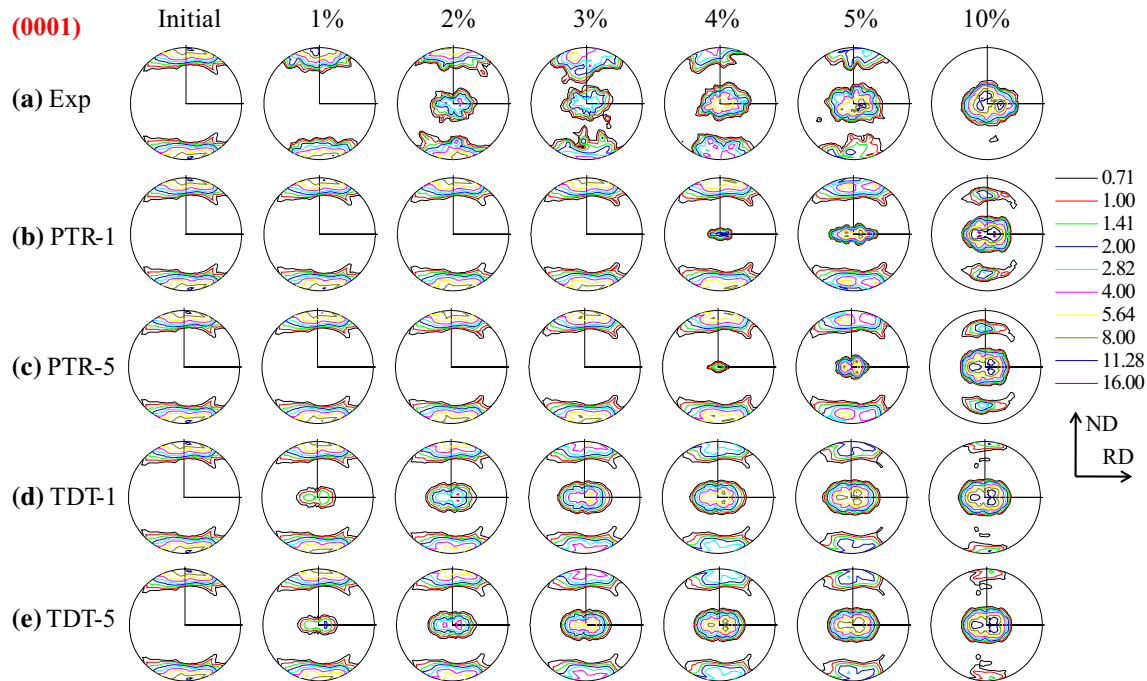


Fig. 7—(0001) pole figures under uniaxial compression along the TD at different strains: (a) measured, (b) EVPSC-PTR- $q=1$, (c) EVPSC-PTR- $q=5$, (d) EVPSC-TDT- $q=1$, and (e) EVPSC-TDT- $q=5$.

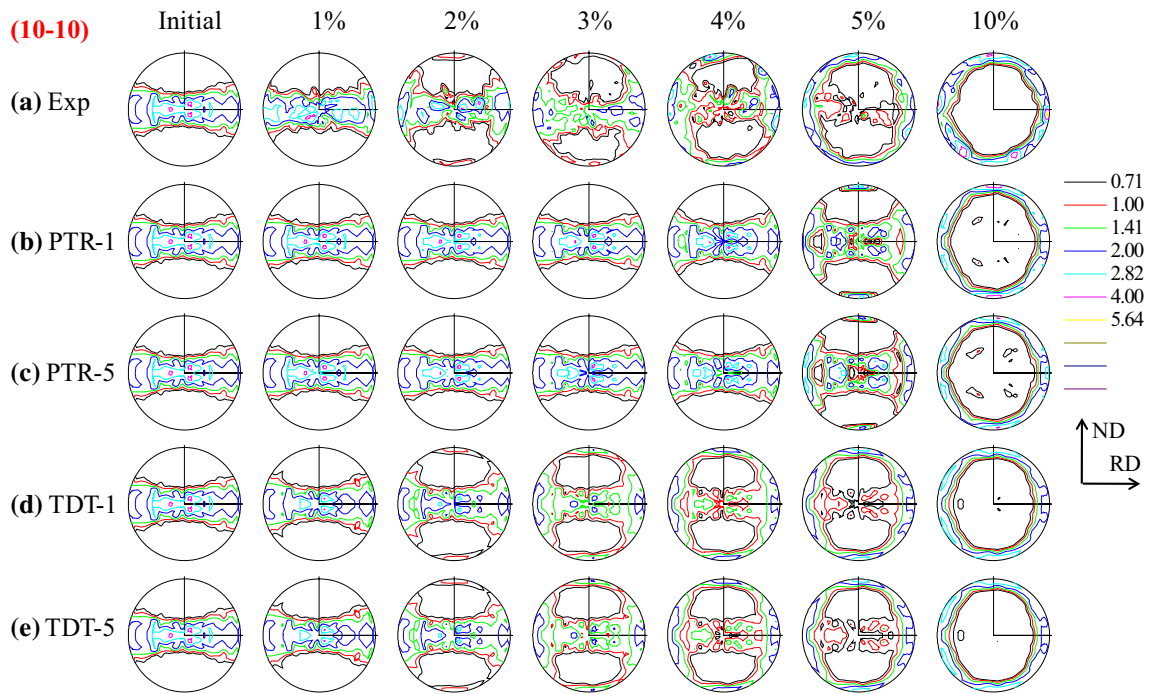


Fig. 8—(10-10) pole figures under uniaxial compression along the TD at different strains: (a) measured, (b) EVPSC-PTR- $q=1$, (c) EVPSC-PTR- $q=5$, (d) EVPSC-TDT- $q=1$, and (e) EVPSC-TDT- $q=5$.

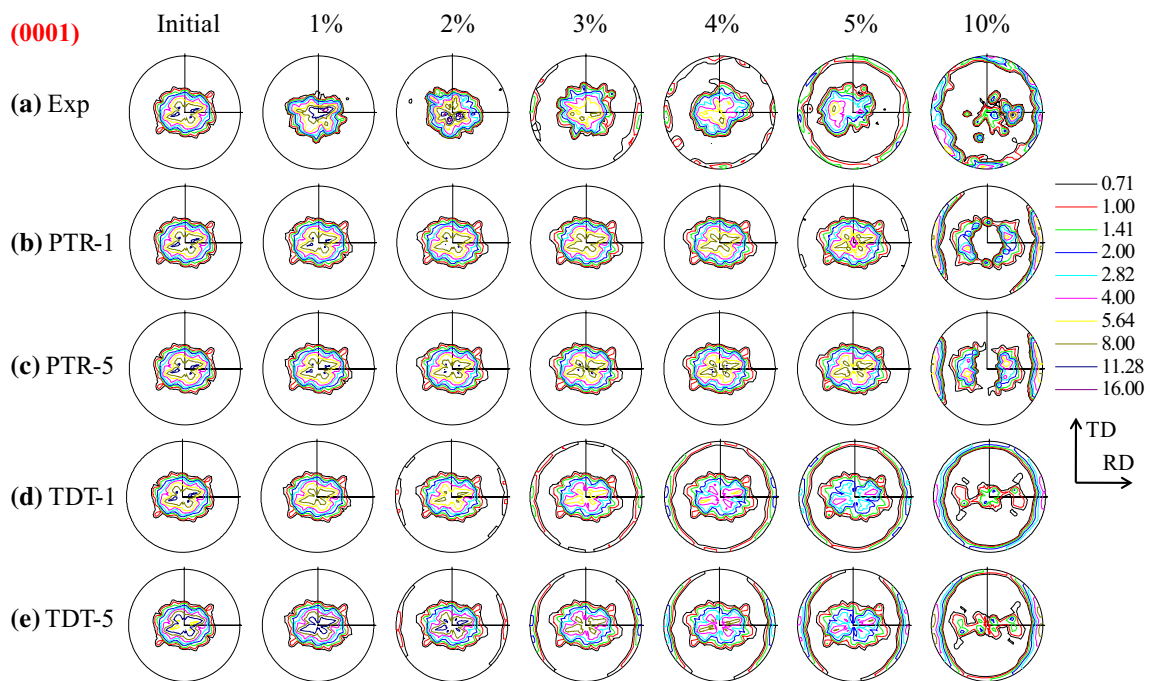


Fig. 9—(0001) pole figures under uniaxial tension along the ND at different strains: (a) measured, (b) EVPSC-PTR- $q=1$, (c) EVPSC-PTR- $q=5$, (d) EVPSC-TDT- $q=1$, and (e) EVPSC-TDT- $q=5$.

and EVPSC-TDT predictions display a texture component in the RD-TD plane, which is stronger close to RD. This component corresponds to the $\{10\bar{1}2\}$ twins. Above $\varepsilon \sim 4$ pct, a minor difference is observed between the simulations with $q = 1$ and $q = 5$. $Q = 1$ makes the

(0001) poles distribute more evenly within the RD-TD plane, whereas with $q = 5$, the (0001) poles lie mainly toward the RD. This difference will be discussed in Section E. Park *et al.*^[58] showed the texture after 2, 5, and 8 pct tensile strain along the ND. In their study, the

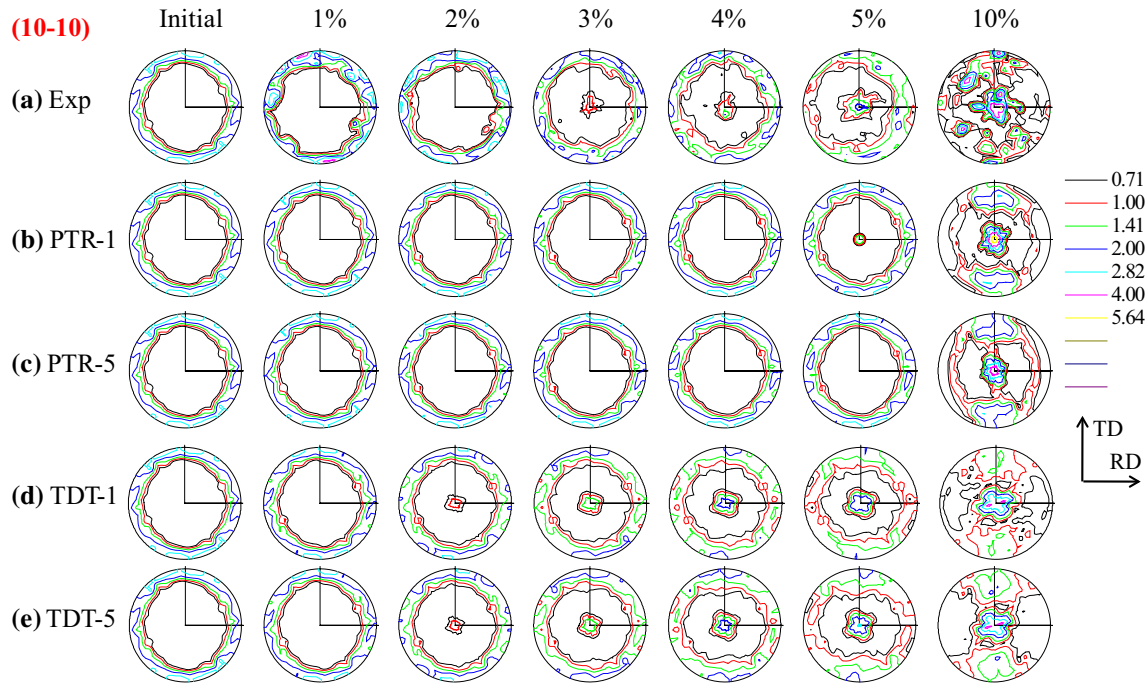


Fig. 10—(10-10) pole figures under uniaxial tension along the ND at different strains: (a) measured, (b) EVPSC-PTR- $q=1$, (c) EVPSC-PTR- $q=5$, (d) EVPSC-TDT- $q=1$, and (e) EVPSC-TDT- $q=5$.

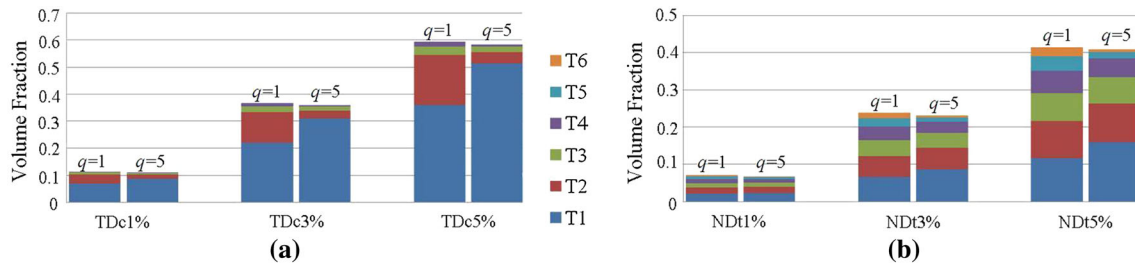


Fig. 11—Twin variants at different strains simulated by the EVPSC-TDT model, with parameters from Table II and $q = 1$ or 5, in (a) TD compression and (b) ND tension.

initial texture was axisymmetric (the (0001) pole figure had no preferential orientation along the TD or RD); after tension, the $\langle c \rangle$ -axes lie in the RD-TD plane, without preferential direction. At $\varepsilon = 10$ pct, a few parent grains retain $\langle c \rangle$ parallel to the ND, whereas the remainder reorient toward the RD. Experimentally, although the measurements are not symmetric, a similar tendency is observed. The $\{10\bar{1}2\}$ twins are responsible for the appearance of the $\{10\bar{1}0\} \parallel \text{ND}$ component visible in Figure 10, while the other $\{10\bar{1}0\}$ components result from the $\langle c \rangle$ -axis orientation.

E. Twin Variant Selection

The effect of q , *i.e.*, the latent hardening, h'' , for $\{10\bar{1}2\}$ twinning by $\{10\bar{1}2\}$ twin systems, is investigated in this section. The effect of q is significant on the simulated stress-strain curves but barely visible on the simulated textures. The twin variants activated in the grains are investigated to explain the effect of q .

The Schmid factor is computed as $P = -s_y n_y$ in TD compression and $P = s_z n_z$ in ND tension (components along $y = \text{TD}$ and $z = \text{ND}$ of the twinning direction, s , and twinning plane, n) so that the most favorable variant has the highest Schmid factor and the highest rank, T1. Figure 11 shows the simulated tension twin variant volume fraction with the EVPSC-TDT model and the two different parameters q , for h'' . The latent-hardening modulus, q , is the only parameter that is changed. As observed previously,^[2,7,39] the variant T1 largely predominates in compression, whereas in tension, all variants are represented. It can be clearly seen that $q = 5$ favors the twin variant T1, whereas lower ranks are disfavored. With $q = 5$, the variant T1 becomes the only significant variant in compression, whereas in tension, the proportion of variant T1 increases moderately and variants T2 through T6 decrease. Also, the effect of $q = 5$ is observed at low strain (1 pct) and the twin-variant volume fractions are proportional to the strain. Although the initial CRSS

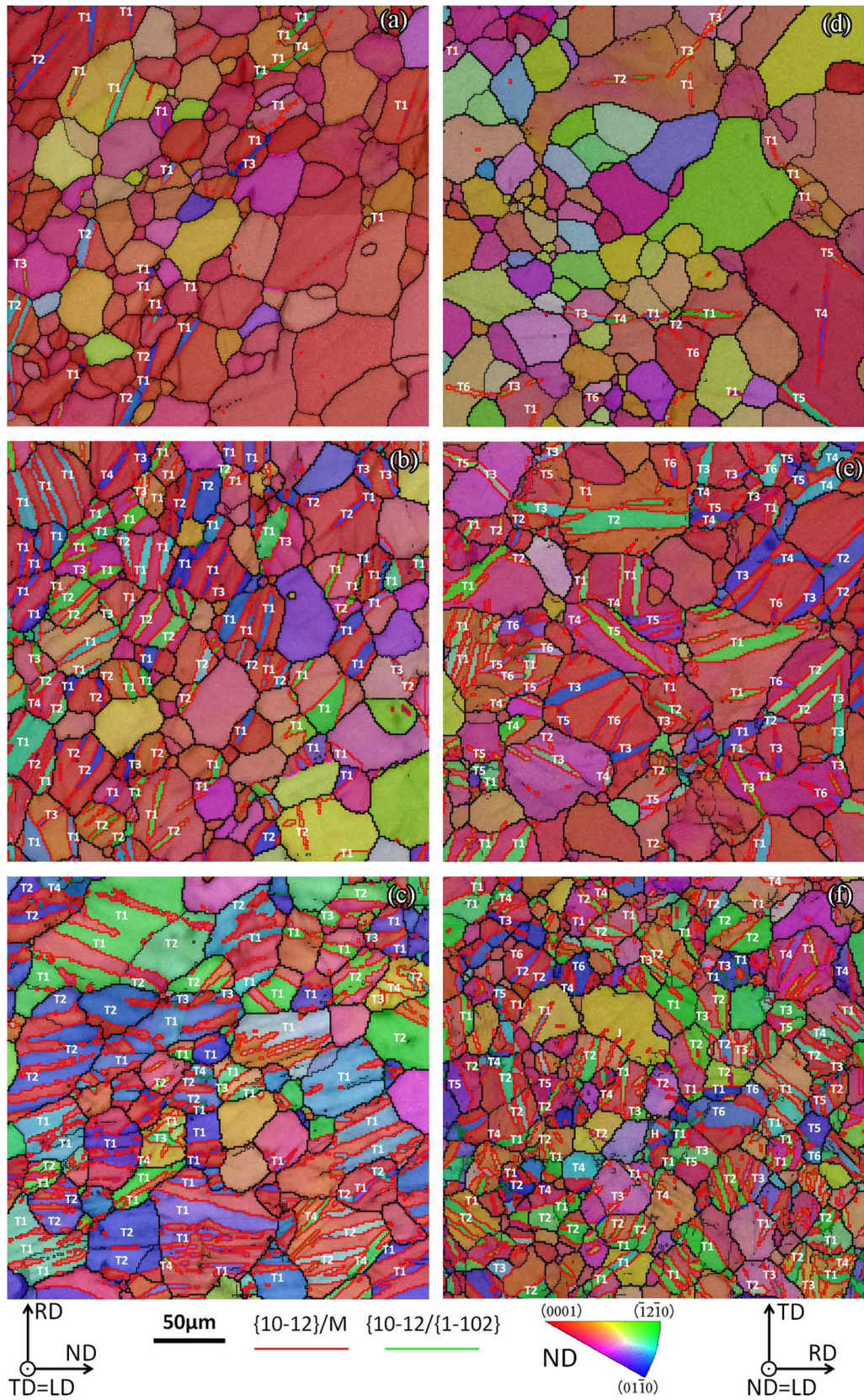


Fig. 12—Detailed EBSD map, with twins identified by their Schmid factor rank for TD compression: (a) 1 pct, (b) 3 pct, (c) 5 pct, and ND tension (d) 1 pct, (e) 3 pct, and (f) 5 pct.

for all twinning systems is the same, it seems that $q = 5$ affects the threshold stress, $\tau_c^{\{10\bar{1}2\}}$, in early deformation and, thus, also the variant selection mechanism during nucleation. This could be explained by Eq. [5].

Tension twin variant analyses were conducted on parts of several EBSD maps (Figure 12). The theoretical orientations of all twin variants were computed from the measured orientations of the remaining (but deformed) parent grains. Since the number of grains with twins is relatively small, no quantitative statistics are presented but a qualitative tendency is observed.

At $\varepsilon = 1$ pct, some areas (Figures 12(a) and (d)) are depleted of twins, illustrating heterogeneous deformation at low strains.^[17] In other areas, twins propagated through grain boundaries, forming cross-boundary twins and twin chains (Figure 12(d)). As expected, the T1 variants are the most observed on all the maps. In TD compression, generally one variant is observed in the grains and, occasionally, two or three. In ND tension, the grains often contain more than one variant and all twin variants are represented. In tension, the variants generally have high and close Schmid factors; hence, a low rank does not always correspond to a low Schmid factor. The variants T1 and T2 rarely belong to the same pair (whereas in compression they often do). At high strains, or when the Schmid factors are close, several variants are identified, but they generally belong to different pairs. Strain compatibility consideration and heterogeneous twin nucleation may explain the occurrence of several low rank twin variants,^[11–15] but a small fraction of them, even in TD-c, are predicted by the EVPSC-TDT model.

At high strains, for TD-c at $\varepsilon = 5$ pct, the Schmid factor analysis is less reliable due to the high deformation; the difference between theoretical and measured twin orientation is often significant (~5 deg). Due to slip, the orientation of the parent grain is no longer the initial orientation; hence, the computed Schmid factor rank could be incorrect, resulting in a reversal in ranks 1 and 2. To evaluate the grain-rotation effect on the twin-variant identification, the simulated twin variants for TD-c at $\varepsilon = 5$ pct were identified using the theoretical grain orientation after deformation (instead of the initial orientation, as in Figure 11): the predictions were very similar, with a somewhat less variant T2 predicted. Thus, the observed variants T2 are potentially not due to the grain rotation.

The variants of rank 2 occur more frequently at higher strains, for TD-c at $\varepsilon = 3$ pct. It is hypothesized that this is not only due to the parent-grain rotation, but also due to inhomogeneous deformation of neighboring grains, which endure different shear strains, resulting in a local shear stress. Hence, the stress field within a grain is different from that of the entire sample (or of the simulated stress field, considering a homogeneous matrix): this type of behavior can only be simulated by CP-FEM models (e.g., References 43 and 59).

In TD compression, the variants T1 and T2 are almost never visible in the same grain, whereas the TDT model frequently predicts them. Although not visible in Figure 11, the simulated twin-variant volume fraction in

each grain does not decrease as the Schmid factor increases from T1 through T6 (e.g., variant T3 could have a higher volume fraction than variant T2) because twin variants must accommodate the strain in three dimensions. The variants T1 and T3, belonging to different pairs, are often observed experimentally. It has been shown that a rate-insensitive Taylor-type model can predict more pairs T1 and T3 than the present rate-sensitive model.^[60] During TD compression, generally one twin variant predominates in each observed grain and the observed variant T2 is potentially due to the heterogeneous stress in the grains that cannot be considered by the model. Hence, in compression, it is reasonable to extensively predict the predominant twin variant T1. Based on the preceding discussion, the EVPSC-TDT model with $q = 5$ provides a better fit with the experimental observations.

IV. CONCLUSIONS

A Mg alloy AZ31 rolled plate was deformed in TD-c and ND-t to different strains, and the texture evolution was measured *via* EBSD. Eight strain paths were used to ascertain the material parameters in the EVPSC-PTR and EVPSC-TDT models. The tension twinning-dominated deformations, *i.e.*, TD compression and ND tension, were systematically investigated using the EVPSC-PTR and EVPSC-TDT models, and the predicted results were compared with experimental data. The following conclusions were reached.

1. The EVPSC-PTR model cannot fit the TD-c and ND-t flow stresses simultaneously, whereas the EVPSC-TDT can. The best-fit parameters for the two models are identical at low strains but diverge moderately at higher strains.
2. A latent-hardening coefficient, h'' , coupling the hardening of each $\{10\bar{1}2\}$ twinning system with others is important to reproduce the flow stresses in both the TD-c and ND-t. An input of $h'' = 5$ significantly increases the CRSS for all $\{10\bar{1}2\}$ variants in the ND-t, but in the ND-c, it keeps the CRSS for the main activated twin variant almost similar to simulations with $h'' = 1$. This latent hardening, $h'' = 5$, permits good reproduction of twin-dominated flow stresses simulated by the EVPSC-TDT model but is not sufficient to fit the flow stresses predicted by the EVPSC-PTR model with the experimental curves.
3. Inputting a high latent hardening for twinning ($h'' = 5$ instead of 1) in the EVPSC-TDT strongly increases the predicted amount of twin variants with the highest Schmid factor (*i.e.*, rank T1) in compression. However, the amount of each twin variant changes moderately in tension.
4. The predicted twin volume fractions are similar based on the two models (with a moderately higher twin volume fraction at high strains in the TDT modeling), but the predicted textures are significantly different. At low strains, none of the grains have twin orientations with parameters input in the

PTR model. The PTR model reproduces the texture above 5 pct strain in the TD-c but cannot reproduce the deformed texture in the ND-t. The TDT model reproduces all the experimental textures.

ACKNOWLEDGMENTS

One of the authors (LZ) is supported by the National Natural Science Foundation of China (Grant Nos. 51571041 and 51421001) and the “111” Project (Grant No. B16007) by the Ministry of Education and the State Administration of Foreign Experts Affairs of China. XG thanks the National Natural Science Foundation of China (Grant No. 51601218) and the Natural Science Foundation of Jiangsu Province (Grant No. BK20160235). PW is supported by the Natural Science and Engineering Research Council of Canada (Grant No. RGPIN-2016-06464).

REFERENCES

- M.R. Barnett: *Mater. Sci. Eng. A*, 2007, vol. 464 (1–2), pp. 1–7.
- S.H. Park, S.-G. Hong, and C.S. Lee: *Scr. Mater.*, 2010, vol. 62 (4), pp. 202–05.
- H. Yu, C. Li, Y. Xin, A. Chapuis, X. Huang, and Q. Liu: *Acta Mater.*, 2017, vol. 128, pp. 313–26.
- S.-G. Hong, S.H. Park, and C.S. Lee: *Acta Mater.*, 2010, vol. 58, pp. 5873–85.
- D.W. Brown, S.R. Agnew, M.A.M. Bourke, T.M. Holden, S.C. Vogel, and C.N. Tomé: *Mater. Sci. Eng. A*, 2005, vol. 399 (1–2), pp. 1–12.
- M. Knezevic, A. Levinson, R. Harris, R.K. Mishra, R.D. Doherty, and S.R. Kalidindi: *Acta Mater.*, 2010, vol. 58 (19), pp. 6230–42.
- X.Q. Guo, A. Chapuis, P.D. Wu, Q. Liu, and X. Mao: *Mater. Des.*, 2016, vol. 98, pp. 333–43.
- S.-G. Hong, S.H. Park, and C.S. Lee: *Scr. Mater.*, 2011, vol. 64 (2), pp. 145–48.
- Y. Pei, A. Godfrey, J. Jiang, Y.B. Zhang, W. Liu, and Q. Liu: *Mater. Sci. Eng. A*, 2012, vol. 550, pp. 138–45.
- B. Wang, R. Xin, G. Huang, and Q. Liu: *Mater. Sci. Eng. A*, 2012, vol. 534, pp. 588–93.
- S. Mu, J.J. Jonas, and G. Gottstein: *Acta Mater.*, 2012, vol. 60 (5), pp. 2043–53.
- C. Guo, R. Xin, C. Ding, B. Song, and Q. Liu: *Mater. Sci. Eng. A*, 2014, vol. 609, pp. 92–101.
- C. Guo, R. Xin, J. Xu, B. Song, and Q. Liu: *Mater. Des.*, 2015, vol. 76, pp. 71–76.
- C. Lou, X. Zhang, and Y. Ren: *Mater. Charact.*, 2015, vol. 107, pp. 249–54.
- Z.-Z. Shi, Y. Zhang, F. Wagner, P.-A. Juan, S. Berbenni, L. Capolungo, J.-S. Lecomte, and T. Richeton: *Acta Mater.*, 2015, vol. 83, pp. 17–28.
- L. Jiang, J.J. Jonas, R.K. Mishra, A.A. Luo, A.K. Sachdev, and S. Godet: *Acta Mater.*, 2007, vol. 55 (11), pp. 3899–3910.
- M.R. Barnett, M.D. Nave, and A. Ghaderi: *Acta Mater.*, 2012, vol. 60 (4), pp. 1433–43.
- P.D. Wu, X.Q. Guo, H. Qiao, and D.J. Lloyd: *Mater. Sci. Eng. A*, 2015, vol. 625, pp. 140–45.
- K. Hazeli, J. Cuadra, P.A. Vanniamparambil, and A. Kontsos: *Scr. Mater.*, 2013, vol. 68 (1), pp. 83–86.
- P. Dobroň, F. Chmelik, S. Yi, K. Parfenenko, D. Letzig, and J. Bohlen: *Scr. Mater.*, 2011, vol. 65 (5), pp. 424–27.
- A. Ghaderi and M.R. Barnett: *Acta Mater.*, 2011, vol. 59 (20), pp. 7824–39.
- O. Muránsky, M.R. Barnett, D.G. Carr, S.C. Vogel, and E.C. Oliver: *Acta Mater.*, 2010, vol. 58 (5), pp. 1503–17.
- R.A. Lebensohn and C.N. Tomé: *Acta Metall. Mater.*, 1993, vol. 41, pp. 2611–24.
- P.A. Turner and C.N. Tomé: *Acta Metall. Mater.*, 1994, vol. 42, pp. 4143–53.
- S.R. Agnew, M.H. Yoo, and C.N. Tomé: *Acta Mater.*, 2001, vol. 49, pp. 4277–89.
- S.R. Agnew and Ö. Duygulu: *Int. J. Plast.*, 2005, vol. 21 (6), pp. 1161–93.
- S.R. Agnew, C.N. Tomé, D.W. Brown, T.M. Holden, and S.C. Vogel: *Scripta Mater.*, 2003, vol. 48 (8), pp. 1003–08.
- H. Wang, P.D. Wu, J. Wang, and C.N. Tomé: *Int. J. Plast.*, 2013, vol. 49, pp. 36–52.
- H. Qiao, P.D. Wu, X.Q. Guo, and S.R. Agnew: *Scr. Mater.*, 2016, vol. 120, pp. 71–75.
- W.B. Hutchinson and M.R. Barnett: *Scr. Mater.*, 2010, vol. 63 (7), pp. 737–40.
- A. Jain and S.R. Agnew: *Mater. Sci. Eng. A*, 2007, vol. 462 (1–2), pp. 29–36.
- H. Wang, B. Raecisina, P.D. Wu, S.R. Agnew, and C.N. Tomé: *Int. J. Solids. Struct.*, 2010, vol. 47 (21), pp. 2905–17.
- Y.B. Chun and C.H.J. Davies: *Mater. Sci. Eng. A*, 2011, vol. 528 (9), pp. 3489–95.
- F. Kabirian, A.S. Khan, and T. Gnäupel-Herlod: *Int. J. Plast.*, 2015, vol. 68, pp. 1–20.
- G. Proust, C.N. Tomé, A. Jain, and S.R. Agnew: *Int. J. Plast.*, 2009, vol. 25 (5), pp. 861–80.
- A.L. Oppedal, H. El Kadiri, C.N. Tomé, G.C. Kaschner, S.C. Vogel, J.C. Baird, and M.F. Horstemeyer: *Int. J. Plast.*, 2012, vols. 30–31, pp. 41–61.
- P.A. Lynch, M. Kunz, N. Tamura, and M.R. Barnett: *Acta Mater.*, 2014, vol. 78, pp. 203–12.
- W. Wu, H. Qiao, K. An, X. Guo, P.D. Wu, and P.K. Liaw: *Int. J. Plast.*, 2014, vol. 62, pp. 105–20.
- C. Ma, A. Chapuis, X.Q. Guo, L. Zhao, P.D. Wu, Q. Liu, and X. Mao: *Mater. Sci. Eng. A*, 2017, vol. 682, pp. 332–40.
- H. Wang, P.D. Wu, C.N. Tomé, and J. Wang: *Mater. Sci. Eng. A*, 2012, vol. 555, pp. 93–98.
- T. Ebeling, C. Hartig, T. Laser, and R. Bormann: *Mater. Sci. Eng. A*, 2009, vol. 527 (1–2), pp. 272–80.
- Z.Q. Wang, A. Chapuis, and Q. Liu: *Trans. Nonferr. Met. Soc.*, 2015, vol. 25 (11), pp. 3595–3603.
- H. Abdolvand and M.R. Daymond: *Acta Mater.*, 2012, vol. 60, pp. 2240–48.
- L.Y. Zhao, A. Chapuis, Y. Xin, and Q. Liu: *J. Alloys Compd.*, 2017, vol. 710, pp. 159–65.
- P. Chen, B. Li, D. Culbertson, and Y. Jiang: *Mater. Sci. Eng. A*, 2017, vol. 709, pp. 40–45.
- H. Wang, P.D. Wu, C.N. Tomé, and Y. Huang: *J. Mech. Phys. Solids*, 2010, vol. 58, pp. 594–612.
- R.A. Lebensohn, C.N. Tomé, and U.F. Kocks: *Acta Metall. Mater.*, 1991, vol. 39, pp. 2667–80.
- A. Chapuis, Z.Q. Wang, and Q. Liu: *Mater. Sci. Eng. A*, 2016, vol. 655, pp. 244–50.
- F. Wang and S.R. Agnew: *Int. J. Plast.*, 2016, vol. 81, pp. 63–86.
- H.H. Yu, Y.C. Xin, M.Y. Wang, and Q. Liu: *J. Mater. Sci. Technol.*, 2018, vol. 34, pp. 248–56.
- J.J. Bhattacharyya, F. Wang, P.D. Wu, W.R. Whittington, H.E. Kadiri, and S.R. Agnew: *Int. J. Plast.*, 2016, vol. 81, pp. 123–51.
- B. Wang, L. Deng, C. Adrien, N. Guo, Z. Xu, and Q. Li: *Mater. Charact.*, 2015, vol. 108, pp. 42–50.
- H. Wang, P.D. Wu, K.P. Boyle, and K.W. Neale: *Int. J. Solids. Struct.*, 2011, vol. 48, pp. 1000–10.
- H. El Kadiri, J. Kapil, A.L. Oppedal, L.G. Hector, S.R. Agnew, M. Cherkaoui, and S.C. Vogel: *Acta Mater.*, 2013, vol. 61 (10), pp. 3549–63.
- O. Muránsky, M.R. Barnett, V. Luzin, and S. Vogel: *Mater. Sci. Eng. A*, 2010, vol. 527 (6), pp. 1383–94.
- J. Wang, I.J. Beyerlein, and C.N. Tomé: *Scr. Mater.*, 2010, vol. 63 (7), pp. 741–46.
- A. Chapuis and Q. Liu: *Comput. Mater. Sci.*, 2015, vol. 97, pp. 121–26.
- S.H. Park, S.-G. Hong, and C.S. Lee: *Scr. Mater.*, 2010, vol. 62 (9), pp. 666–69.
- H. Qiao, M.R. Barnett, and P.D. Wu: *Int. J. Plast.*, 2016, vol. 86, pp. 70–92.
- A. Chapuis, Y. Xin, X. Zhou, and Q. Liu: *Mater. Sci. Eng. A*, 2014, vol. 612, pp. 431–39.